Available online at www.sciencedirect.com
ScienceDirect
Theoretical Population Biology 71 (2007) 1–11
Theoretical Population Biology
www.elsevier.com/locate/tpb

Nonlinear dynamics and pattern bifurcations in a model for vegetation stripes in semi-arid environments

Jonathan A. Sherratt*, Gabriel J. Lord

Department of Mathematics and Maxwell Institute, Heriot-Watt University, Edinburgh EH14 4AS, UK

Received 4 January 2006
Available online 16 September 2006

Abstract

In many semi-arid environments, vegetation is self-organised into spatial patterns. The most striking examples of this are on gentle slopes, where striped patterns are typical, running parallel to the contours. Previously, Klausmeier [1999. Regular and irregular patterns in semiarid vegetation. Science 284, 1826–1828.] has proposed a model for vegetation stripes based on competition for water. Here, we present a detailed study of the patterned solutions in the full nonlinear model, using numerical bifurcation analysis of both the pattern ODEs and the model PDEs. We show that patterns exist for a wide range of rainfall levels, and in particular for much lower rainfall than have been considered by previous authors. Moreover, we show that for many rainfall levels, patterns with a variety of different wavelengths are stable, with mode selection dependent on initial conditions. This raises the possibility of hysteresis, and in numerical solutions of the model we show that pattern selection depends on rainfall history in a relatively simple way.

Keywords: Vegetation patterns; Tiger bush; Hysteresis; Rainfall history

1. Introduction

In many semi-arid environments, vegetation is not homogeneous, but rather is self-organised into spatial patterns. On flat ground, these patterns have a seemingly random appearance, but on gentle slopes, a striped pattern is typical, with bands of vegetation up to 250 m wide, separated by gaps of up to 1 km, running along the contours. These patterns occur in a wide range of grasses and small shrubs. They are hard to detect on the ground, and were first observed in aerial photographs of sub-Saharan Africa in the 1950s (MacFadyen, 1950; Hemming, 1965; Wickens and Collier, 1971). Subsequently, vegetation patterns have also been found in Australia (Mabbutt and Fanning, 1987; Dunkerley and Brown, 2002) and Mexico (Montaña et al., 1990; Montaña, 1992).

Competition for water and the positive feedback between water availability and plant growth are widely recognised as the underlying cause of vegetation patterning. However, the details of the process remain unclear, and have been subject to a number of mathematical modelling studies. This paper is concerned with the modelling approach of Klausmeier (1999), who synthesised ideas in earlier computer-based simulation models (Thiéry et al., 1995; Mauchamp et al., 1994; Dunkerley, 1997) to give coupled differential equations for vegetation $U(x,t)$ and surface water $W(x,t)$:

$$\partial U/\partial T = \overbrace{k_1 U^2 W}^{\text{plant growth}} - \overbrace{k_2 U}^{\text{plant loss}} + \overbrace{k_3 \partial^2 U/\partial X^2}^{\text{dispersal}}, \tag{1a}$$

$$\partial W/\partial T = \underbrace{k_4}_{\text{rainfall}} - \underbrace{k_5 W}_{\text{evaporation}} - \underbrace{k_6 U^2 W}_{\text{uptake by plants}} + \underbrace{k_7(\partial W/\partial X)}_{\text{flow downhill}}. \tag{1b}$$

Here $k_1,\ldots,k_7$ are positive constants. These equations represent the basic processes of plant growth in proportion to water availability, plant loss, and plant dispersal. Water input is due to rainfall, and water is lost through a combination of evaporation and active uptake by plants. This last term is nonlinear in the plant density U because the presence of plant roots in the soil increases water

*Corresponding author.
E-mail addresses: jas@macs.hw.ac.uk (J.A. Sherratt), gabriel@macs.hw.ac.uk (G.J. Lord).

0040-5809/$ - see front matter © 2006 Elsevier Inc. All rights reserved.
doi:10.1016/j.tpb.2006.07.009

infiltration (Rietkerk et al., 2004). The spatial coordinate X runs uphill, so that there is an active flow of water in the negative X direction. Klausmeier (1999) showed that numerical simulations of (1) do predict vegetation stripe formation, for appropriate parameters; a typical solution is illustrated in Fig. 1. Intuitively, these patterns arise because rainfall onto an area without vegetation will run downhill, facilitating plant growth in the adjacent region of vegetation on the downhill side. An appropriate balance is required between water input to a vegetation band and water loss/uptake, and this determines the possible widths of the bands and gaps. Intuitively, one expects that the moist soil on the uphill side of a stripe will create a tendency for the stripes to migrate uphill. Such movement is indeed observed in simulations of the Klausmeier model, and has been reported in some field studies (Worrall, 1959; Hemming, 1965; Montaña, 1992). However, this remains a controversial aspect of vegetation patterns, due in part to the very slow speed of the predicted migrations—typically it would take about 100 years for the pattern to move a single wavelength.

The Klausmeier (1999) model is focussed on water flow downhill, and does not predict patterning on flat ground ($k_7 = 0$). However Rietkerk, van de Koppel and coworkers have subsequently proposed a number of models that

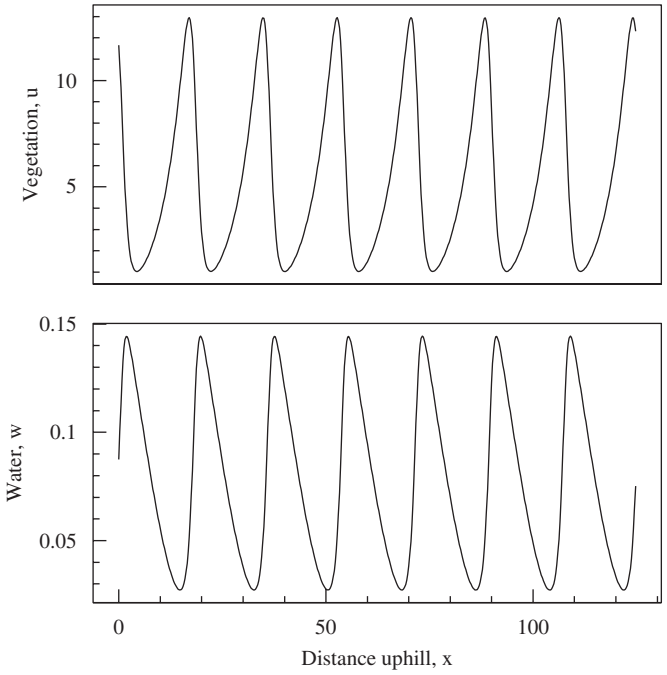

Fig. 1. An illustration of a typical vegetation pattern, as predicted by the Klausmeier model (2). There is a periodic pattern of peaks in vegetation density u, separated by regions in which vegetation is almost absent. The surface water density w also has a periodic form; it is largest on the uphill side of a vegetation stripe, and gradually decreases with distance uphill to the next stripe. The pattern moves slowly uphill; in this case the (dimensionless) migration speed is approximately 0.9. The parameter values are $A = 2.5$, $B = 0.45$, $v = 182.5$, which are in the range of Klausmeier's (1999) parameter estimates for grass. The equations were solved numerically (see text) on the domain $0 < x < 125$ with periodic boundary conditions.

incorporate an additional variable, as well as plant density and surface water. In (HilleRisLambers et al., 2001), this group added a separate variable for water within the soil, and Rietkerk et al. (2002) performed a detailed numerical bifurcation study on a minor variant of this model, showing that the bifurcations leading to patterning are subcritical. Similarly, van de Koppel et al. (2002) added a variable for herbivores. These models predict patterns on flat ground as well as on hillsides, and can be regarded as more realistic extensions of the Klausmeier (1999) model.

The Klausmeier model and its extensions are not the only theoretical explanation for vegetation stripes. Lejeune and coworkers (Lefever and Lejeune, 1997; Lejeune and Tlidi, 1999; Couteron and Lejeune, 2001; Lejeune et al., 2004) have studied in detail a model based on the combination of short-range activation and long-range inhibition between neighbouring plants. Here the activation is due to shading of one plant by another, while competition for water results in inhibition; the difference in length scales of these processes is due to the root system within the soil being much more extensive than the parts of the plants above ground. In this model, slope acts as a selector rather than an initiator of spatial patterning. Meron and coworkers (von Hardenberg et al., 2001; Meron et al., 2004) take yet another approach, with a model formulated in terms of plant density and water in the soil, in which the latter has a transport term based on porous media theory. More recently, the same group has proposed a related model with separate variables for surface water and soil water (Gilad et al., 2004). Again, these models predict pattern formation on flat as well as sloping ground.

At a superficial level, the Klausmeier, Rietkerk-van de Koppel, Lejeune and Meron models all provide plausible explanations for vegetation patterning. Therefore, a full understanding of patterning in the various models is essential for distinguishing the different mechanisms, and our objective in this paper is to develop such an understanding for the Klausmeier model.

The natural first step in studying pattern formation in (1) is to use linear analysis to study low amplitude patterns. Sherratt (2005) has presented a detailed study of this type and the results are summarised in Section 2. In Section 3, we present numerical results to which these analytical approximations can be compared. We show from numerics that patterned solutions exist for significantly smaller rainfall levels than previously considered. Our approach involves applying the bifurcation package AUTO (Doedel, 1981; Doedel et al. 1991a,b) to the ordinary differential equations governing patterned solutions. This bifurcation and stability approach has some similarities with that of Rietkerk et al. (2002); however the patterns generated by their model are stationary, which gives considerable simplification. In contrast, the patterns we are studying move uphill, and the speed of this movement enters as an additional parameter in our calculations. Our work in Section 3 indicates possible patterns as a function the speed of this migration; however, it gives no information about

the crucial question of whether patterns are stable in the model PDEs (1). In Section 4 we address this via a different approach that is much more intensive computationally: we apply AUTO to a discretised version of the PDEs from which we obtain a prediction of linear stability. Finally, in Section 5 we discuss the mathematical and ecological implications of our results.

2. Linear analysis

The model equations (1) are greatly simplified by the following non-dimensionalisation

$$u = Uk_6^{1/2}/k_5^{1/2}, \quad w = Wk_1/k_5^{1/2}k_6^{1/2},$$
$$x = Xk_5^{1/2}/k_3^{1/2}, \quad t = Tk_5,$$
$$A = k_4k_1/k_5^{3/2}k_6^{1/2}, \quad B = k_2/k_5, \quad v = k_7/k_3^{1/2}k_5^{1/2}.$$

These rescalings are taken from Klausmeier (1999), although our notation is different. The resulting dimensionless equations are

$$\partial u/\partial t = wu^2 - Bu + \partial^2 u/\partial x^2, \tag{2a}$$

$$\partial w/\partial t = A - w - wu^2 + v\partial w/\partial x. \tag{2b}$$

In applications, the main dimensional parameters of interest are the rainfall k_4, plant loss k_2 and gradient of slope k_7; note that plant loss will vary depending on the extent of grazing. These three parameters appear (linearly) in the dimensionless quantities A, B and v, respectively. Therefore, in the remainder of the paper we study the dimensionless equations (2), focussing on the conditions for patterning, and the way in which the patterns vary with these three parameters. An indication of the typical values of these parameters is given by Klausmeier's (1999) estimates, which are for trees (rainfall) $A \in [0.077, 0.23]$, (plant loss) $B = 0.045$, and for grass $A \in [0.94, 2.81]$, $B = 0.45$; in both cases $v = 182.5$ for a typical slope with vegetation stripes.

For all parameter values, (2) has a stable trivial steady state $u = 0$, $w = A$, corresponding to bare ground, without vegetation. When $A \geqslant 2B$, there are also two other homogeneous steady states which arise from a saddle node bifurcation

$$u = u_1 \equiv \frac{2B}{A + \sqrt{A^2 - 4B^2}}, \quad w = w_1 \equiv \frac{A + \sqrt{A^2 - 4B^2}}{2} \tag{3}$$

and

$$u = u_2 \equiv \frac{2B}{A - \sqrt{A^2 - 4B^2}}, \quad w = w_2 \equiv \frac{A - \sqrt{A^2 - 4B^2}}{2}. \tag{4}$$

The first of these (3) is always unstable to homogeneous perturbations; the second is the key equilibrium from which patterns develop. This steady state is linearly stable to homogeneous perturbations whenever $B < 2$. For larger values of B and small A, (4) can become unstable, giving complicated local dynamics including a limit cycle, but realistic parameter values for semi-arid environments imply that $B < 2$. The linear stability analysis presented in (Sherratt, 2005) then shows that for some parameter values, (4) is unstable to spatially inhomogeneous perturbations, giving rise to pattern formation. Sherratt (2005) was unable to obtain an exact condition for instability, but did derive an approximation to the condition, namely

$$v > \sqrt{8}A^2/B^{5/2} \tag{5}$$

which gives an approximate upper limit on the rainfall A for pattern formation. Both Klausmeier (1999) and Sherratt (2005) assumed that a corresponding lower limit was given by the condition $A > 2B$ for the uniform vegetation state to exist. However, in this paper we show that stable patterned solutions may exist for $A < 2B$.

The basis for the approximation used to derive (5) is the large (dimensionless) value of v in comparison to A and B; recall that Klausmeier (1999) estimates $v = 182.5$ for a typical slope with vegetation stripes, which compares with $A \in [0.077, 0.23]$, $B = 0.045$ for trees, and $A \in [0.94, 2.81]$, $B = 0.45$ for grass. To understand the intuitive interpretation of (5), recall that A reflects the rainfall, while B is a measure of plant loss, and v indicates the steepness of the slope. If the rainfall A is too small compared to plant loss B, then vegetation will simply die out. On the other hand, if rainfall A is sufficiently large, then the competition amongst plants for water will not be very strong, resulting in homogeneous vegetation. However, for intermediate levels of rainfall, vegetation can survive but with a strong competition amongst plants for water, leading to vegetation stripes. The dependence of the upper threshold on v occurs because on steeper slopes rainfall will run off more quickly, increasing the competitive advantage of areas of high plant density over those of lower density. However the whole model assumes that the slope is not too steep, otherwise the water will not flow downhill as a sheet, and instead will form gullies.

3. Existence and properties of pattern solutions

From an ecological viewpoint, a key issue is the dependence on parameters of the wavelength and uphill migration speed of vegetation stripes. Sherratt (2005) studied this question in detail by assuming that the patterns correspond to the most unstable wavenumber. This will be valid sufficiently close to the onset of patterning, but numerical simulations suggest more complicated dependencies for larger amplitude patterns. The basic objective of this paper is to investigate pattern form, selection, and dependence on parameters in the fully nonlinear regime. Our numerical analysis suggests that (2) does not have any stationary patterns, with the homogeneous steady states being the only stationary solutions. Instead, the patterns move at a constant speed, so that they have the mathematical form $u(x, t) = U(z)$,

and $w(x,t) = W(z)$, where $z = x - ct$ and c is the migration speed; the patterns are periodic travelling wave solutions. Substituting these solution forms into (2) gives the ODEs

$$d^2U/dz^2 + c\,dU/dz + WU^2 - BU = 0, \tag{6a}$$

$$(v + c)\,dW/dz + A - W - WU^2 = 0. \tag{6b}$$

In this section we investigate numerically the existence, speed and wavelength of patterns. Our approach is to use the bifurcation package AUTO (Doedel, 1981; Doedel et al. 1991a,b) to study the pattern ODEs (6). To do this, the most natural bifurcation parameter is the wave speed c. In the partial differential equation model (2), the wave speed is a model output, dependent on the model parameters and on the initial and boundary conditions, but in (6) the speed enters explicitly as an independent parameter. Because the system (6) is third order, computations are rapid, but they give no information about the stability of patterns as solutions of the model PDEs (2); that question is addressed in Section 4.

Our starting point is the homogeneous steady state (4). When $c = 0$ this steady state is stable, but provided v is sufficiently large, the stability changes as c is increased, via a Hopf bifurcation of (6). The periodic solutions that emanate from this Hopf bifurcation are the slowly moving patterns corresponding to vegetation stripes, where the spatial wavelength is the period. As c is increased beyond the Hopf point, the steady state (4) is at first unstable, but regains stability through a second Hopf bifurcation. Note that here we use the terms "stable" and "unstable" as referring to the ODE system (6) rather than the model PDE. There is no relationship between the stability of solutions in one system and the stability in the other.

Typical bifurcation diagrams are illustrated in Fig. 2, which shows that for moderate values of v the patterns form a single branch that links the two Hopf points (Fig. 2a). However a gap develops as v is increased, giving two separate branches with an intermediate range of speeds for which there are not any pattern solutions (Fig. 2b). Careful investigation shows that the gap is formed by bifurcations to two homoclinic orbits with different wave speeds c. The slower homoclinic orbit is homoclinic to the trivial steady state $u = 0$, $w = A$ whereas the faster homoclinic orbit is homoclinic to the steady state (u_2, w_2). This is illustrated by plots of pattern wavelength against speed c in Figs. 2c and d, which use the same parameter

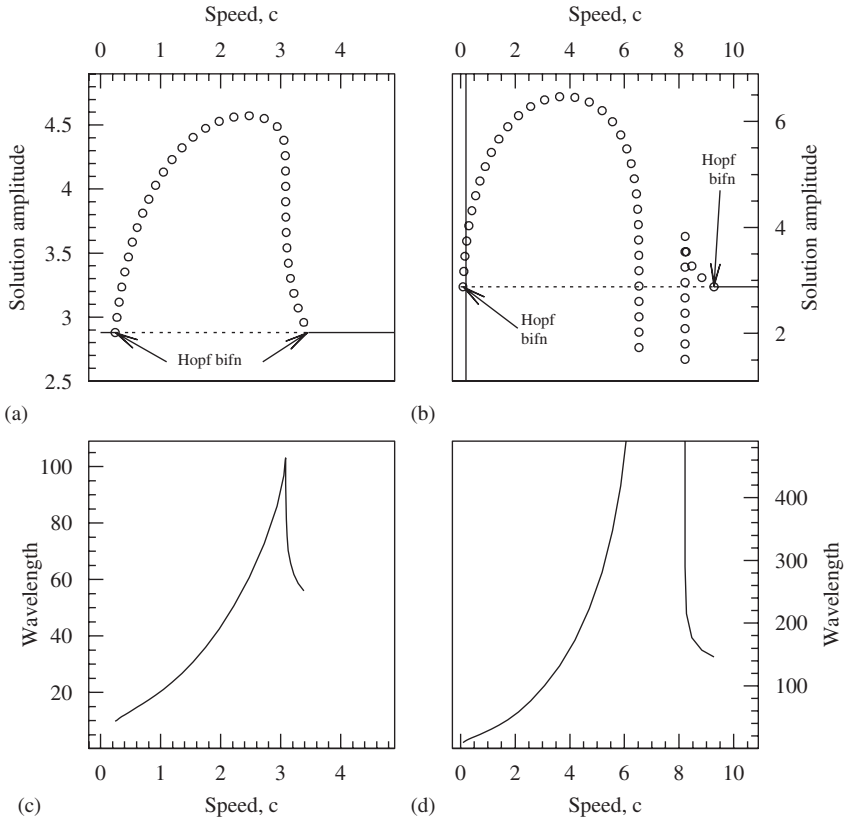

Fig. 2. Typical bifurcation diagrams for the pattern ODEs (6). The homogeneous steady state (4) is stable (—-) for very small and for large values of the speed c, but unstable (- - - -) at intermediate values of c. The changes in stability occur via Hopf bifurcations, from which a branch of periodic orbits (○ ○ ○) emanate; these are the vegetation stripe patterns. At moderate values of the slope v as in (a), the periodic orbits form a single solution branch, but for larger v as in (b), there are two separate branches, both of which terminate in homoclinic solutions. Parts (c) and (d) show the wavelength along the periodic orbit branches; the wavelengths tend to infinity at the ends of the two separate branches, reflecting the homoclinic orbits. The parameter values are: (a), (c) $A = 1.45$, $B = 0.45$, $v = 70$; (b), (d) $A = 1.45$, $B = 0.45$, $v = 182.5$. Note that the stability shown in the bifurcation diagram refers to the travelling wave ODEs (6) rather than the PDEs (2).

values as Figs. 2a and b, respectively. For the moderate value of v used in Figs. 2a and c, the wavelength initially increases with c, reaches a maximum, and then decreases; however in Fig. 2d the wavelength tends to infinity at both edges of the gap in the bifurcation diagram.

Using AUTO, it is possible to track the locus of both the Hopf bifurcation points and the homoclinic solutions in a parameter plane, and a typical example of this for the v–c plane is illustrated in Fig. 3a. As v is decreased, the two Hopf bifurcation points move towards one another and eventually meet, so that the locus of Hopf points is in fact a single curve. The minimum value of v along this curve corresponds to the condition (5) for pattern formation. The locus of homoclinic orbits lies inside the locus of Hopf points; again the speeds of the two homoclinic solutions come together as v is decreased, at a bifurcation of higher co-dimension (seen as the cusps in Fig. 3). Patterned solutions exist for values of c and v lying in between these two loci. Using AUTO, it is also possible to track the loci of patterns with a particular wavelength, and a typical example is shown in Fig. 3a. The curve emanates from the locus of Hopf bifurcations, and approaches $c = 0$ asymptotically as $v \to \infty$. Note that the loci of homoclinic orbits shown in Fig. 3 are in fact approximations given by the loci of solutions of a fixed but very long wavelength (3000).

The corresponding loci are shown for the B–c and A–c planes in Figs. 3b and c, respectively. The basic structure is the same, except that in both cases, all three loci have an additional fold at very small values of c. Fig. 3d shows a more comprehensive series of loci of patterns of fixed wavelength, for the same parameters as in Fig. 3c. Note that for any given value of the migration speed c, intermediate levels of both plant loss B and rainfall A are required for patterns. If plant loss is too high, or rainfall is too low, vegetation cannot survive; this edge of the parameter region giving patterns is bounded by the homoclinic orbit curve. Conversely if plant loss is too low or rainfall too high, competition for water is weak and vegetation is spatially homogeneous; here the parameter region giving patterns is bounded by the Hopf bifurcation curve. The maximum value of rainfall A required for patterning is exactly as predicted by linear analysis (Sherratt, 2005), and corresponds to the steady state (u_2, w_2) becoming unstable to inhomogeneous perturbations. However, the minimum value, which corresponds to the fold in the locus of homoclinic orbits to $(0, A)$, is significantly less than that assumed by previous authors

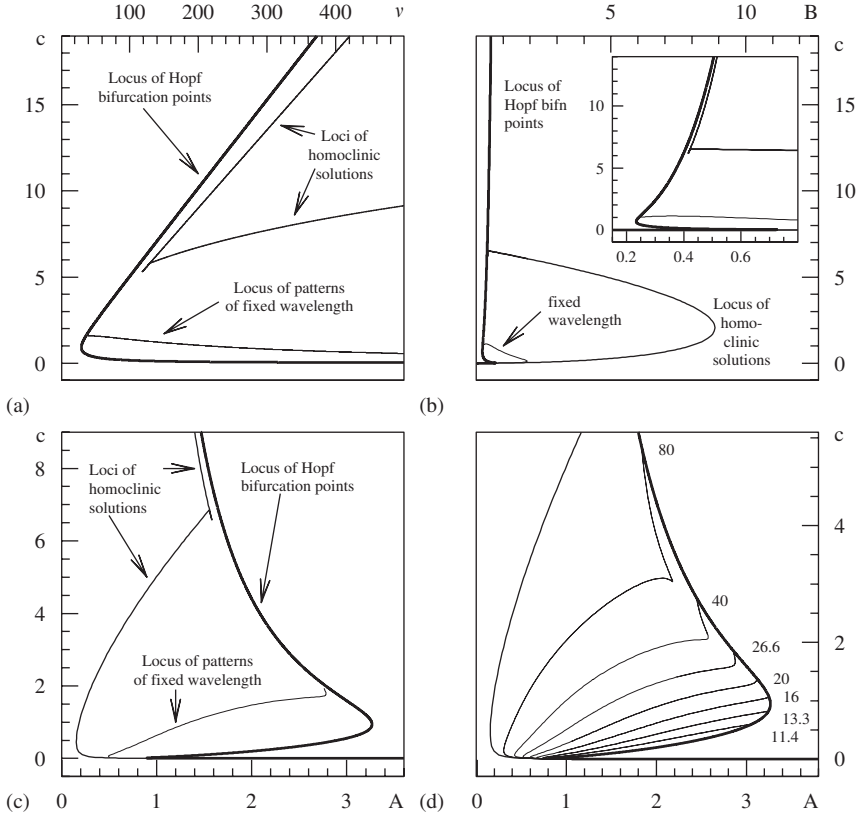

Fig. 3. An illustration of the variations in parameter space of the solution structure of the pattern ODEs (6). We plot the loci of Hopf bifurcation points ——, homoclinic solutions —— and patterns of fixed wavelength —— in the (a) v–c, (b) B–c and (c), (d) A–c planes. In (a)–(c) the value of the wavelength along the dashed curve is 30; in (d) a number of different wavelengths are used, with values shown at the ends of the branches. In (b), we show a close-up of behaviour for small B, which is unclear in the main part of the figure. The values of the fixed parameters are: (a) $A = 1.45$, $B = 0.45$; (b) $A = 1.45$, $v = 182.5$; (c), (d) $B = 0.45$, $v = 182.5$.

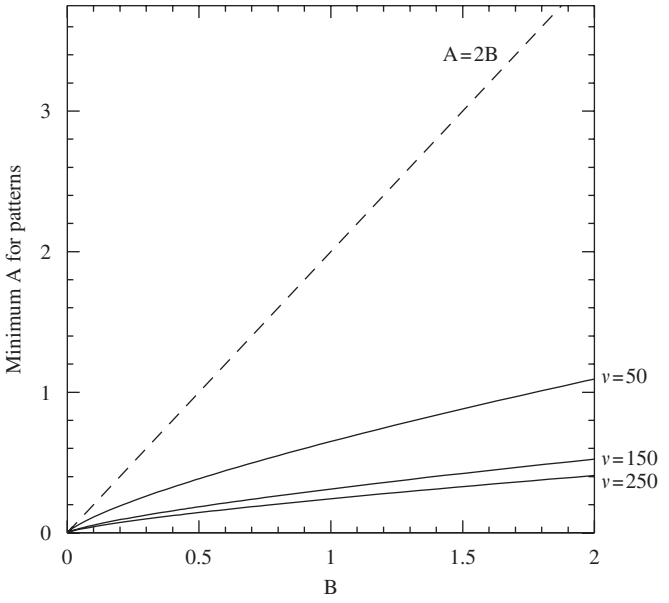

Fig. 4. A plot of the minimum level of rainfall A that is required for vegetation patterning, as a function of the two other dimensionless parameters B and v, which correspond to the rate of plant loss and the steepness of the slope, respectively. We plot the minimum A as a function of B for three different values of v (50, 150 and 250). In previous studies of the model (1) (Klausmeier, 1999; Sherratt, 2005), it has been assumed that the minimum value of A for patterns is the same as the minimum value for the homogeneous equilibrium (4), which is $2B$ (independent of v). This is shown as a dashed line in the figure, demonstrating that in fact, patterns exist for much lower levels of rainfall. The minimum value of A is calculated by a numerical continuation of the lower fold in the locus of homoclinic orbits in the A–c plane (see Fig. 3c); this locus is the lower bound on A for known patterned solutions of a given speed, and therefore the fold gives the lower bound for the existence of patterned solutions of any speed.

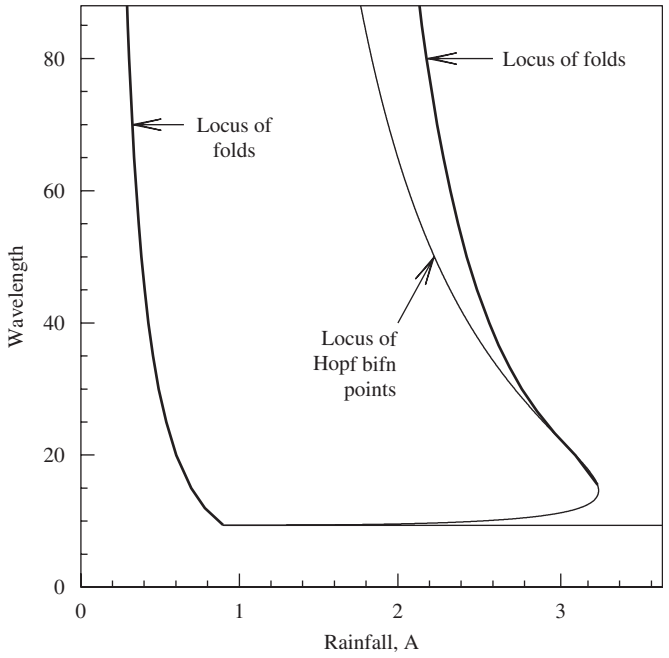

Fig. 5. An illustration of the range of wavelengths over which patterns exist, as a function of A. The parameters are the same as in Fig. 3d, and this figure is most easily understood by reference to Fig. 3d. The plots of speed vs A for fixed wavelength, shown in Fig. 3d, have two folds when the wavelength is greater than about 15, and a single fold for smaller wavelengths; the thick lines in this figure are the loci of these folds. The thin line is the locus of Hopf bifurcation points. The region in which pattern solutions exist is bounded by the two loci of folds, and the portion of the Hopf point locus that connects them.

(Klausmeier, 1999; Sherratt, 2005), namely the value of A ($= 2B$) below which (u_2, w_2) does not exist. This is illustrated more clearly in Fig. 4.

This figure shows that in fact, patterns exist for A as low as about $0.2B$ for a wide range of B and v. Moreover, our investigation of stability (below) suggests that throughout this large range, there are patterns that are stable as solutions of the original model (2).

It is possible to convert the values of A shown in Fig. 4 into dimensional rainfall levels, using the parameter estimates of Klausmeier (1999).[1] These imply that the minimum levels of rainfall for vegetation patterns is 45 mm year^{-1} for grass and 100 mm year^{-1} for trees, which are broadly consistent with the lowest rainfalls at which vegetation patterning has been reported (Tongway and Ludwig, 2001).

From parameter space plots such as those shown in Fig. 3, it is possible to deduce the range of possible wavelengths for pattern solutions, as a function of the model parameters. As a specific case, we consider the wavelengths as a function of the rainfall parameter A. Fig. 3d shows that for a fixed and sufficiently large wavelength, the maximum possible value of A for which there is a pattern is given by the right-hand fold in the locus of patterns of fixed wavelength. For smaller wavelengths (less than about 15), there is no such fold, and the maximum A lies on the locus of Hopf bifurcation points. In either case, the minimum possible A is given by the left-hand fold in the locus of patterns of fixed wavelength. Tracing loci of the folds using AUTO gives the wavelength-A parameter plane shown in Fig. 5. This figure shows that when the rainfall is relatively small (A less than about 2.2), there is a wide range of possible wavelengths, but as A increases above this level the range of wavelengths rapidly shrinks, until patterns disappear entirely at $A \approx 3.27$.

4. Stability of pattern solutions

The results of Section 3 give a detailed understanding of the existence of patterned solutions, as a function of the model parameters A, B and v and the migration speed c. However, because we have been studying the travelling

[1]The details of Klausmeier's (1999) parameter estimation are mainly contained in footnote 21 of the paper. In this footnote, there is an error associated with the units. Klausmeier's dimensional parameter R should have units of m^4 year^{-1} (kg dry mass)$^{-2}$, not (kg water)m^2 year^{-1}(kg dry mass)$^{-2}$.

wave ODEs (6), we have not been able to determine the stability of the patterns as solutions of the model equations (2). Determination of periodic travelling wave stability, even numerically, is a notoriously difficult problem (Sandstede, 2002). We have taken the approach of discretising the PDEs (2) in space, applying upwinding to the convective term, to give a system of coupled ODEs:

$$\partial u_i/\partial t = w_i u_i^2 - Bu_i + (u_{i+1} - 2u_i + 2u_{i-1})/\Delta x^2, \tag{7a}$$

$$\partial w_i/\partial t = A - w_i - w_i u_i^2 + v(w_{i+1} - w_i)/\Delta x \tag{7b}$$

$(i = 1, \ldots, N)$. For simplicity, we assume periodic boundary conditions $u_0(t) = u_N(t)$, $w_0(t) = w_N(t)$, $u_{N+1}(t) = u_1(t)$, $w_{N+1}(t) = w_1(t)$. We studied system (7) using the bifurcation package AUTO, with the objective of recovering bifurcation diagrams such as those shown in Fig. 3, but with additional information about pattern stability.

For any discretisation that is sufficiently fine to be of practical use, (7) is a large system of equations, and studying patterned solutions using AUTO is a major computational challenge. Therefore, we have focussed on pattern variation with just one of the three parameters, the rainfall A, with the values of B and v fixed at 0.45 and 182.5, respectively. We have used $N = 40$, which gives 80 equations in (7), with a spatial grid length $\Delta x = 2$. This gives a discrete representation of the model equations on a domain of length 80, which is large enough to capture a range of pattern behaviour; for a more accurate representation we would use a smaller value of Δx and a larger value of N, but the problem quickly exceeds computational feasibility.

For a sufficiently large value of A, there are no patterned solutions and the homogeneous steady state $u_i = u_2$, $w_i = w_2$ $(i = 1, \ldots, N)$ is stable as a solution of (7). As A is decreased, the steady state becomes unstable via a Hopf bifurcation at $A \approx 3.05$ (Fig. 6). The branch of periodic solutions emanating from this Hopf bifurcation is spatially as well as temporally periodic, with a wavelength of 8 space points (i.e. a spatial wavelength of 16). This is a mode 5 pattern. As the branch is continued, both A and the speed gradually decrease until a fold at $A \approx 0.75$, after which A then increases. As A approaches infinity, the speed approaches zero, while the amplitude tends to a non-zero finite limit. Note that the wave speed is not now a

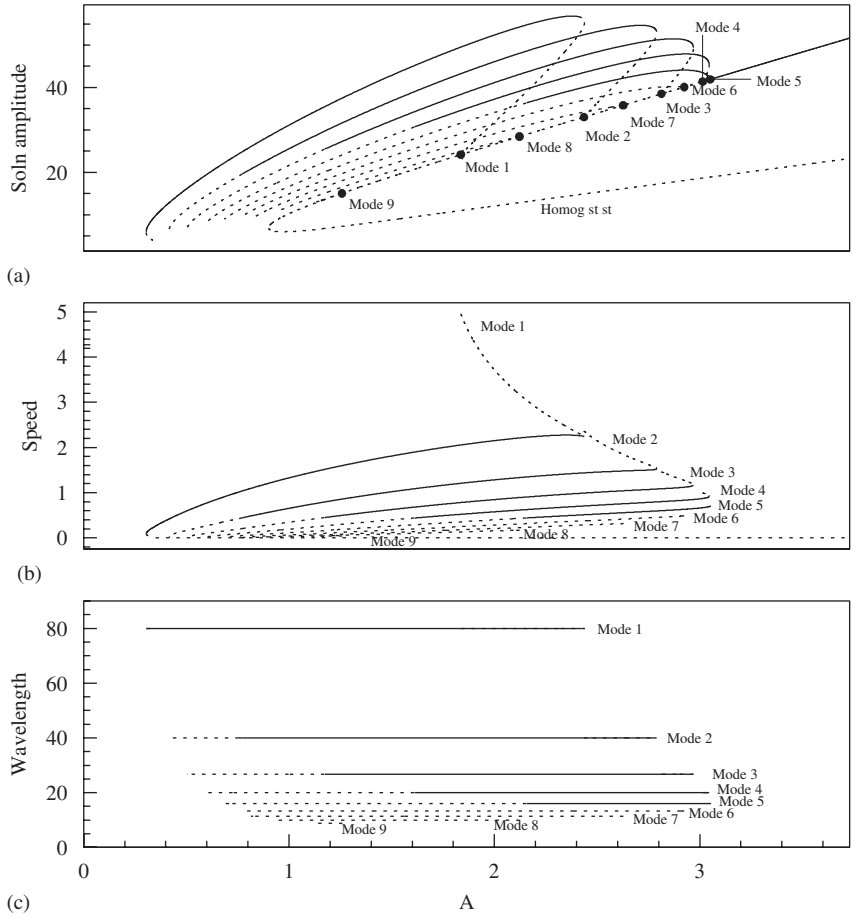

Fig. 6. Bifurcation diagrams of pattern solutions in the discretised model equations (7). Solid lines correspond to stable solutions and dashed lines correspond to unstable solutions. We plot: (a) solution amplitude; (b) speed and (c) wavelength as a function of the rainfall parameter A, with $B = 0.45$, $v = 182.5$, $N = 40$ and $\Delta x = 2$. The solution branches with different spatial modes arise via separate Hopf bifurcations. In (a) we also show the amplitude of the homogeneous steady state from which the spatial pattern branches bifurcate. In (a) and (b) the mode 9 branch is plotted, but is barely visible.

parameter in system (7), but rather is a property of the solution, calculated as the ratio of the space and time periods. This solution branch is the discrete analogue of the locus of patterns of wavelength 16 that is plotted in Fig. 3d. However, because (7) is a representation of the PDEs, AUTO calculates not only the solution branch but also its linear stability as a solution of a large system of ODEs. This shows that these mode 5 patterns are stable for A greater than about 2.15, and are unstable for smaller values of A.

As A is decreased further, the homogeneous steady state $u_i = u_2,\ w_i = w_2\ (i = 1, \ldots, N)$ undergoes another Hopf bifurcation at $A \approx 3.01$. In this case the branch of periodic solutions consists of mode 4 patterns, with a wavelength of 10 space points (i.e. a spatial wavelength of 20). Again this is a discrete analogue of the locus of patterns of wavelength 20 shown in Fig. 3d. In this case the Hopf bifurcation is subcritical and A initially increases on the branch, with a fold at $A \approx 3.05$. The patterns are initially unstable, and gain stability at this fold. Both A and the wave speed then decrease along the branch, with a loss of stability at $A \approx 1.6$. There is then a further fold at $A \approx 0.6$ after which A increases again with the speed approaching zero.

Decreasing A still further, the homogeneous steady state undergoes a series of additional Hopf bifurcations. At each of these, a branch of periodic solutions emanates, corresponding to a pattern of a particular spatial mode. For our parameter set, the order at which the bifurcations occur is mode 5 first, then modes 4, 6, 3, 7, 2, 8, 1 and 9 successively; it is straightforward to predict this order via linear stability analysis (details omitted for brevity). We have not detected any Hopf bifurcations for values of A below the bifurcation at $A \approx 1.26$, which corresponds to the mode 9 branch. Of course, system (7) cannot have solutions with an exact spatial mode of 6, 3, 7 or 9 because these are not divisors of the number of equations ($N = 40$). Strictly, the solutions on these branches have a spatial period of 40 points. Nevertheless they are approximately periodic in space with quasi-periods of 40/6, 40/3, 40/7 and 40/9, respectively, and we interpret them as discrete analogues of the corresponding branches of periodic travelling waves. This correspondence can be made precise via linear stability analysis using the eigenvectors of the discretised Laplacian. Typical spatial variations of solutions on the various branches is illustrated in Fig. 7. Within the context of our coarse discretisation, the solutions on the mode 6–9 branches are all unstable, while the mode 1–5 branches all have regions of stability and regions of instability.

In Fig. 6 we illustrate the behaviour described above with a bifurcation diagram for (7), plotted in three different ways: the parameter A against: (a) solution amplitude; (b) wave speed, and (c) spatial wavelength. The plots in (b) and (c) are the discrete analogues of Figs. 3d and 5, respectively. The qualitative comparison between the figures is very good, despite the relative coarseness of the discretisation. The additional information available in Fig. 6 concerns stability, showing that there are stable

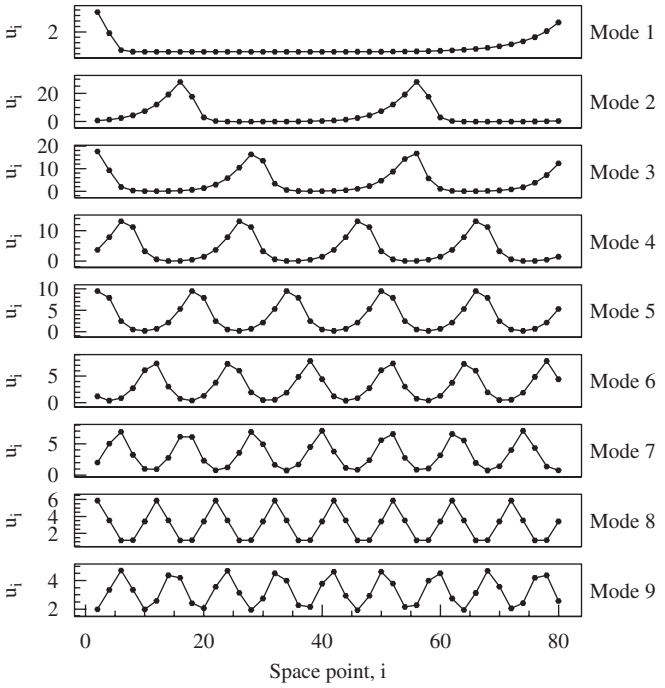

Fig. 7. Typical spatial profiles of the solutions of the discretised version of the PDE (7) on the various solution branches. We plot u_i against i at one time point. All of the solutions are for $B = 0.45$ and $v = 182.5$, with $A = 1.5$ for modes 1–8, and $A = 1.114$ for mode 9. For modes 1, 2, 4, 5 and 8 the solutions have spatial periodicity corresponding to the mode number, while for modes 3, 6, 7 and 9 the periodicity is approximate.

patterns across the full range of values of A for which patterns exist, and moreover that for many values of A, several different spatial modes are stable.

To investigate the implications of the coexistence of different stable pattern modes, we solved the discretised PDEs (7) numerically as an initial value problem. For time stepping we used both VODE (Brown et al., 1989; García-Archilla, 1995), which is a variable coefficient solver, and MATLAB `ode23s` specifying the Jacobian and absolute and relative error tolerances of 10^{-6} and 10^{-3}, respectively. We deliberately used the same coarse discretisation as for Figs. 6 and 7, so that we could expect an exact match between the solutions of the initial value problem and the solutions predicted by AUTO. We used initial conditions consisting of small random perturbations about one of the two homogeneous steady states (u_2, w_2) and (u_1, w_1), defined in (4) and (3), respectively. For values of A for which several different pattern modes are stable, we expect different perturbations of the steady states to evolve to different patterns, and this is confirmed by our simulations, which are illustrated in Fig. 8. For each value of $A = 0.1, 0.2, \ldots, 3.4$, we ran 100 simulations, using different seeds for the random initial perturbations. In each case, the solutions evolved either to a spatial pattern of mode 1–5, or to a homogeneous steady state. This last possibility is denoted by the wavelength being zero in the figure, and the corresponding steady state is (u_2, w_2) when $A > 3$, and the desert state $(0, A)$ when $A < 0.9$. The distribution of

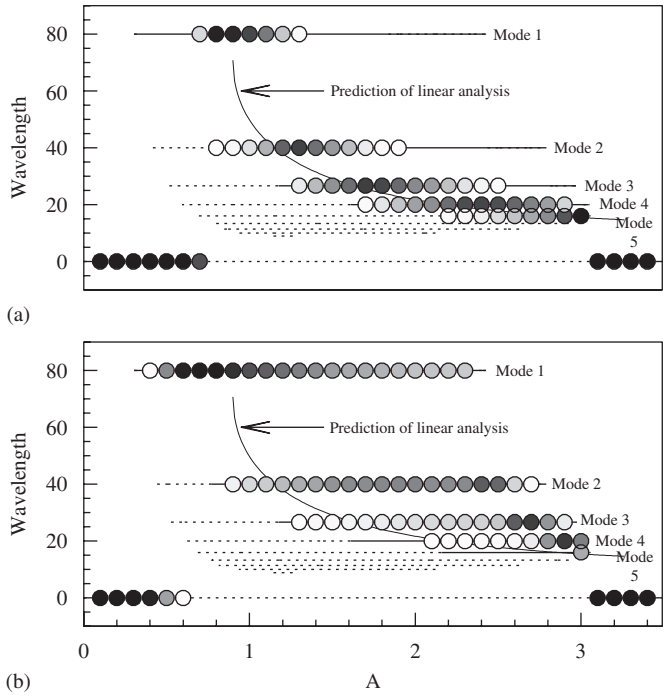

Fig. 8. An illustration of the dependence of pattern selection on initial conditions for the discretised model equations (7). We plot pattern wavelength vs the rainfall parameter A, with solid and dotted horizontal lines showing the wavelength of patterns that are stable and unstable, respectively; these are the same in (a) and (b), and the same as in Fig. 6c. Superimposed on this is the pattern wavelength that evolves from initial conditions that are small random perturbations of the uniform steady states (a) (u_2, w_2) and (b) (u_1, w_1). In all cases, the initial conditions evolve either to a homogeneous steady state, for which the wavelength is shown as zero, or to a pattern of mode 1–5. For each value of $A = 0.1, 0.2, \ldots, 3.4$, we have run 100 simulations, using different seeds for the random number generator used in the initial conditions. The patterns selected by these initial conditions are indicated by circles, with the interior of the circles showing frequency of selection in greyscale (darker = higher frequency). We also plot the variation of wavelength with A that is predicted by linear stability analysis. Pattern wavelength is tightly clustered around this curve in (a), but is significantly different in (b). The parameter values are $B = 0.45$, $v = 182.5$, $N = 40$ and $\Delta x = 2$. The specific form of the initial conditions is: (a) $u_i = R_i u_2$, $v_i = S_i w_2$, (b) $u_i = R_i u_1$, $v_i = S_i w_1$, where R_i and S_i are chosen randomly from a uniform distribution between 0.9 and 1.1.

solutions between the possible outcomes is illustrated by greyscale shading, with darker shading indicating a higher frequency of pattern selection. Thus a circle with a white interior indicates that only one out of the 100 initial conditions developed into a pattern of that particular wavelength, whereas a circle with a black interior indicates that all of the initial conditions generated that pattern. Our results show that the observed spatial pattern does indeed depend on the initial conditions. When the initial conditions involve perturbations about (u_2, w_2), the observed wavelengths are clustered around those predicted by linear stability analysis (Fig. 8a); this is because pattern selection occurs while the solutions are still of low amplitude, so that the linearised equations are a good approximation to the full system. The same clustering does not occur when the initial conditions involve perturbations around the unstable (and so unphysical) solution (u_1, w_1) (Fig. 8b).

The clustering of pattern wavelength around the most linearly unstable mode is important because in applications, patterns will most commonly develop from spatially homogeneous vegetation, for example due to a drop in rainfall or an increase in grazing. We investigated this clustering as domain length increased, and found that it is remarkably pronounced even on relatively large domains. We took as a particular example the case of $N = 160$, again with $\Delta x = 2$: this is a coarse discretisation of a domain of length 320. Linear analysis predicts that the most unstable pattern is mode 12 in this case. We ran 1000 simulations with initial conditions consisting of small perturbations to the steady state (u_2, w_2). Of these runs, 42.9% evolved to mode 12 patterns and 47.2% to mode 11 or mode 13 patterns. Of the remainder, 4.5% evolved to mode 10 or mode 14 patterns, and 5.4% did not converge to a periodic pattern within our allocated solution time (which was 4800). This finding of persistent clustering around the most unstable mode as domain length is increased implies that the distribution of pattern wavelength becomes progressively sharper.

Our finding that multiple pattern modes are unstable for many parameter sets raises the interesting possibility of hysteresis. To investigate this, we returned to the original model PDEs (2), solving numerically using a much finer discretisation than for (7). We imposed a variation in the rainfall parameter A over time, as illustrated in Fig. 9; the parameter values and domain length are the same as in Figs. 3 and 5. Initially the system is at the spatially uniform steady state (u_2, w_2), with A sufficiently large that this is stable. As A is decreased, a pattern develops that is mode 5, as expected from our results in Section 5. A further decrease in A causes a change in the qualitative form of the pattern but the wavelength remains the same: the solution moves along the solution branch consisting of mode 5 patterns. The smallest value of A used in Fig. 9 is too low for stable mode 5 patterns (see Fig. 5), and the pattern changes to mode 1. But as A is increased again, the mode 5 pattern does not reappear. Rather, the solution moves to the mode 3 branch and continues on this until the homogeneous steady state is retrieved. Note that the parameter values used in Fig. 9 are based on estimates for grass derived by Klausmeier (1999), and these imply that the range $A \in [0.5, 3.5]$ used in the figure corresponds to rainfall levels between about 130 and 930 mm year^{-1}.

5. Discussion

Wavelength is the most accessible property of vegetation stripes in the field. It requires observation at only a single time and moreover this can be done via aerial photography, avoiding the logistical difficulties and expense of ground-based study. Therefore, the most important prediction of theoretical models for vegetation stripes is

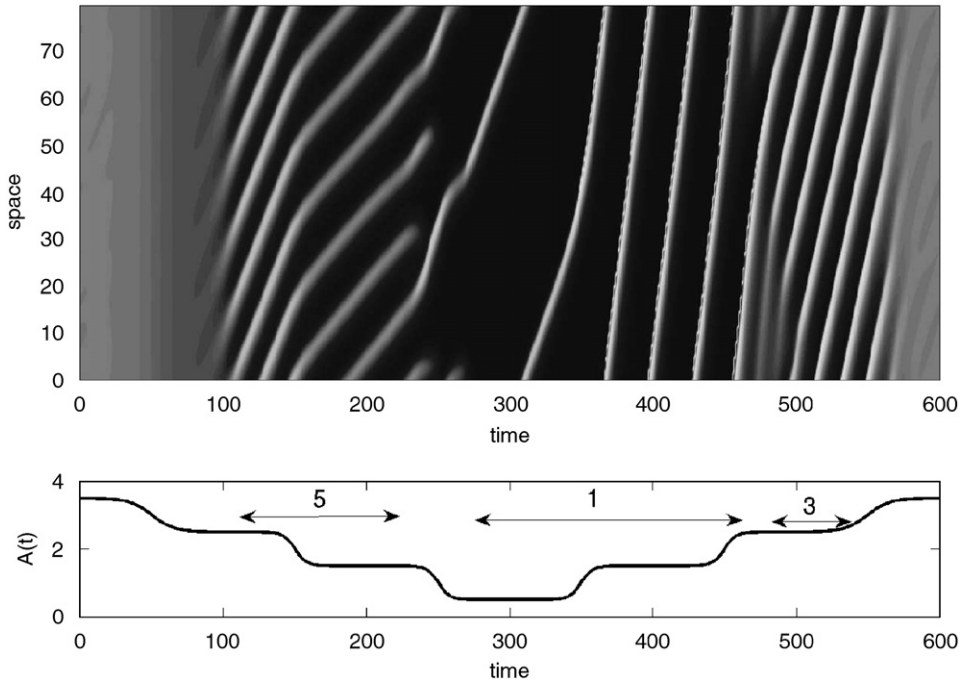

Fig. 9. An illustration of hysteresis in the full model PDEs (2) as the rainfall is varied. In the upper panel, we plot vegetation density as a function of space and time in grey scale (dark = low density, light = high density). In the lower panel we show the rainfall parameter A, which has an imposed variation in time, rather than being constant. We also indicate the mode number of the corresponding vegetation pattern. Initially A is sufficiently large that there are no vegetation patterns, and the stable solution is spatially uniform vegetation $u = u_2$, $w = w_2$. We use this as the initial condition in our simulation. As A is decreased, a mode 5 pattern emerges; this is expected by reference to Fig. 3 and 6, which show that the initial bifurcation to patterns gives a mode 5 solution. As A is decreased further to 1.5, the mode 5 pattern persists but changes its form. Note that Fig. 6 indicates that the mode 5 pattern is unstable for this value of A, but for the finer discretisation we are using here it is stable. Finally, A is decreased sufficiently that the mode 5 solution loses stability and the solution changes to a mode 1 pattern, which is the only stable patterning mode at low values of A (see Fig. 6). As A is increased again, the solution remains on the mode 1 branch until this loses stability, when a mode 3 pattern develops. This persists until A is increased back to its original value, when homogeneous vegetation is restored. The critical feature of this figure is that although the decrease and increase in A are symmetric, the change in vegetation patterns is highly asymmetric. The system of 400 ODEs resulting from the finite difference approximation (with $\Delta x = 0.2$) was solved using MATLAB (see text).

pattern wavelength and its variation with model parameters.

For the Klausmeier (1999) model, linear stability analysis of the uniform vegetation state reveals the stability of different spatial wavenumbers, and previous authors (Klausmeier, 1999; Sherratt, 2005) have made predictions on pattern wavelength based on the most unstable wavenumber. Our results show that it is wrong to make this simple assumption that the observed pattern has the most unstable wavenumber. Rather, pattern selection is nonlinear and history-dependent. To be specific, we have focussed on patterning in response to changes in rainfall, although analogous results hold for changes in grazing levels.

Vegetation stripes can be initiated either by the destabilisation of the homogeneous vegetation state, or by the introduction of plants to desert regions. In the former case, the Klausmeier model predicts a critical rainfall level at which pattern formation occurs; linear stability analysis enables calculation of this critical level, and also the corresponding spatial wavelength (Sherratt, 1999). Our results show that as rainfall is further decreased, pattern wavelength remains the same, although the form of the pattern changes gradually, with the vegetation stripes becoming thinner and the stripe separation increasing. The pattern wavelength only changes at a rainfall level that is significantly less than that at which patterns first arise—by a factor of 0.7 for the specific parameter set on which we focussed in Section 4. In comparison, the most unstable wavelength changes by about 30% during this change in rainfall. Once pattern wavelength does finally increase, the longer wavelengths persist even when rainfall increases again (see Fig. 9).

Patterns that might arise via the introduction of plants to desert areas cannot be studied using the stability and bifurcation approach used in this paper, because the desert steady state is always linearly stable in the Klausmeier model, so that even with high rainfall it requires a large perturbation to get vegetation growth. However, our results in Fig. 8 indicate that at the lowest rainfall levels allowing patterns, these will have mode 1, so that there is a single vegetation stripe on the domain, whatever its size. This is confirmed by numerical simulations of the model PDEs (2), which show that for any rainfall level for which a mode 1 pattern exists, introduction of plants to a desert area always generates this pattern unless the plants die out.

At high rainfall levels, the mode 1 patterns become unstable (see Fig. 8), and large perturbations of the desert state then generate shorter wavelength patterns. If the rainfall is then decreased again these patterns persist, in a manner analogous to the hysteresis shown in Fig. 9.

In conclusion, our results show that pattern selection in the Klausmeier (1999) model differs significantly from the "most unstable mode" rule assumed by previous authors. Moreover, our work enables predictions of pattern wavelength based on parameter values and on a basic knowledge of rainfall history. In the context of a parameterisation of the model for a particular vegetation system, such predictions could be used to test the validity of the Klausmeier (1999) model.

Acknowledgments

JAS was supported in part by an Advanced Research Fellowship from EPSRC. We thank Olivier Lejeune for helpful discussions.

References

Brown, P.N., Byrne, G.D., Hindmarsh, A.C., 1989. VODE: a variable coefficient ODE solver. SIAM J. Sci. Stat. Comput. 10, 1038–1051.

Couteron, P., Lejeune, O., 2001. Periodic spotted patterns in semi-arid vegetation explained by a propagation-inhibition model. J. Ecol. 89, 616–628.

Doedel, E.J., 1981. AUTO, a program for the automatic bifurcation analysis of autonomous systems. Cong. Numer. 30, 265–384.

Doedel, E.J., Keller, H.B., Kernévez, J.P., 1991a. Numerical analysis and control of bifurcation problems: (I) Bifurcation in finite dimensions. Int. J. Bifurcation Chaos 1, 493–520.

Doedel, E.J., Keller, H.B., Kernévez, J.P., 1991b. Numerical analysis and control of bifurcation problems: (II) Bifurcation in infinite dimensions. Int. J. Bifurcation Chaos 1, 745–772.

Dunkerley, D.L., 1997. Banded vegetation: development under uniform rainfall from a simple cellular automation model. Plant Ecol. 129, 103–111.

García-Archilla, B., 1995. Some practical experience with the time integration of dissipative equations. J. Comput. Phys. 122, 25–29.

Gilad, E., von Hardenberg, J., Provenzale, A., Shachak, M., Meron, E., 2004. Ecosystem engineers: from pattern formation to habitat creation. Phys. Rev. Lett. 93, 098105.

Hemming, C.F., 1965. Vegetation arcs in Somaliland. J. Ecol. 53, 57–67.

HilleRisLambers, R., Rietkerk, M., van de Bosch, F., Prins, H.H.T., de Kroon, H., 2001. Vegetation pattern formation in semi-arid grazing systems. Ecology 82, 50–61.

Klausmeier, C.A., 1999. Regular and irregular patterns in semiarid vegetation. Science 284, 1826–1828.

Lefever, R., Lejeune, O., 1997. On the origin of tiger bush. Bull. Math. Biol. 59, 263–294.

Lejeune, O., Tlidi, M., 1999. A model for the explanation of vegetation stripes. J. Vegetation Science 10, 201–208.

Lejeune, O., Tlidi, M., Lefever, R., 2004. Vegetation spots and stripes: dissipative structures in arid landscapes. Int. J. Quantum Chem. 98, 261–271.

Mabbutt, J.A., Fanning, P.C., 1987. Vegetation banding in arid Western Australia. J. Arid Environ. 12, 41–59.

MacFadyen, W., 1950. Vegetation patterns in the semi-desert plains of British Somaliland. Geographical J. 115, 199–211.

Mauchamp, A., Rambal, S., Lepart, J., 1994. Simulating the dynamics of a vegetation mosaic: a spatialized functional model. Ecol. Model. 71, 107–130.

Meron, E., Gilad, E., von Hardenberg, J., Shachak, M., Zarmi, Y., 2004. Vegetation patterns along a rainfall gradient. Chaos Solitons Fractals 19, 367–376.

Montaña, C., 1992. The colonization of bare areas in two-phase mosaics of an arid ecosystem. J. Ecol. 80, 315–327.

Montaña, C., Lopez-Portillo, J., Mauchamp, A., 1990. The response of two woody species to the conditions created by a shifting ecotone in an arid ecosystem. J. Ecol. 78, 789–798.

Rietkerk, M., Boerlijst, M.C., van Langevelde, F., HilleRisLambers, R., van de Koppel, J., Prins, H.H.T., de Roos, A., 2002. Self-organisation of vegetation in arid ecosystems. Am. Nat. 160, 524–530.

Rietkerk, M., Dekker, S.C., de Ruiter, P.C., van de Koppel, J., 2004. Self-organised patchiness and catastrophic shifts in ecosystems. Science 305, 1926–1929.

Sandstede, B., 2002. Stability of travelling waves. In: Handbook of Dynamical Systems II. North-Holland, Amsterdam, pp. 983–1055.

Sherratt, J.A., 2005. An analysis of vegetation stripe formation in semi-arid landscapes. J. Math. Biol. 51, 183–197.

Thiéry, J.M., D'Herbès, J.-M., Valentin, C., 1995. A model simulating the genesis of banded vegetation patterns in Niger. J. Ecol. 83, 497–507.

Tongway, D.J., Ludwig, J.A., 2001. Theories on the origins, maintainance, dynamics, and functioning of banded landscapes. In: Tongway, T.J., Valentin, C., Seghieri, J. (Eds.), Banded Vegetation Patterning in Arid and Semiarid Environments. Springer, New York.

van de Koppel, J., Rietkerk, M., van Langevelde, F., Kumar, L., Klausmeier, C.A., Fryxell, J.M., Hearne, J.W., van Andel, J., de Ridder, N., Skidmore, M.A., Stroosnijder, L., Prins, H.H.T., 2002. Spatial heterogeneity and irreversible vegetation change in semiarid grazing systems. Am. Nat. 159, 209–218.

von Hardenberg, J., Meron, E., Shachak, M., Zarmi, Y., 2001. Diversity of vegetation patterns and desertification. Phys. Rev. Lett. 87, (198101).

Wickens, G.E., Collier, F.W., 1971. Some vegetation patterns in the Republic of Sudan. Geoderma 6, 43–59.

Worrall, G.A., 1959. The Butana grass patterns. J. Soil Sci. 10, 34–53.